Revealing the hydrogenation performance of RuMo phosphide for chemoselective reduction of functionalized aromatic hydrocarbons

Yolanda Bonita, Timothy P. O'Connell, Holly E. Miller, and Jason C. Hicks*

Department of Chemical and Biomolecular Engineering, University of Notre Dame, 182 Fitzpatrick Hall, Notre Dame, Indiana 46556, United States

*Corresponding author's email: jhicks3@nd.edu

Abstract

Bimetallic transition metal phosphide catalysts are promising materials for low temperature, liquid phase hydrogenation reactions. This work explores the chemoselective hydrogenation ability of RuMoP using various functionalized aromatic hydrocarbons to provide insight into how the functional groups compete for reduction on the surface of RuMoP. Using molecular hydrogen as the reductant, high selectivity (~99%) to reduction of the substituent is achieved for the hydrogenation of electron withdrawing functionalities such as nitrobenzene, benzaldehyde, and benzophenone with RuMoP to yield aniline, benzyl alcohol, and diphenylmethanol, respectively. In contrast, aromatics with electron donating groups such as phenol, anisole, and toluene, show high ring hydrogenation selectivity (~99%) to form cyclohexanol, methoxycyclohexane, and methyl cyclohexane, respectively, although the reaction proceeded slowly with RuMoP. Pyridine adsorption was studied via diffuse reflectance infrared Fourier transform spectroscopy (DRIFTS), which provided evidence of surface electron deficient sites (i.e., Lewis acids) that are responsible for targeting the electron rich portion of the substrate. Additional DRIFTS experiments were performed using nitrobenzene, anisole, and a mixture of the two. From these experiments, features associated with -NO_2 adsorption in nitrobenzene and ring adsorption in anisole were observed, which correlated well with the observed reaction results. Finally, a solvent study provided evidence for the competitive adsorption of isopropanol and the π-electrons from the aromatic ring of phenol with the former being more favorable on RuMoP surface.

1. Introduction

Selective hydrogenation reactions are highly important chemical transformations for the production of chemicals and the upgrading of lignocellulosic biomass.[1] As one pertinent example, functionalized aniline compounds are derived from the reduction of nitroaromatic hydrocarbons and are useful chemicals as pharmaceuticals, agrochemicals, and dyes.[2-7] In the case of biomass upgrading, liquid bio-oils produced from either pyrolysis or liquefaction of lignocellulosic biomass are comprised of aromatic hydrocarbons with a variety of different functionalities such as aldehydes, ketones, esters, and phenolic sustituents.[8-10] The existence of aromatic and oxygenated species in the molecules provides multiple functional groups that can compete for adsorption sites on the catalysts. Therefore, an understanding of how newly discovered catalysts interact with molecules containing multiple functionalities is warranted.

Many catalysts such as supported Au, Pd, Pt, and Ru have been studied for hydrogenation reactions of compounds with multiple functionalities such as nitro aromatics, aromatic rings, and carbonyls.[11-19] Another material that is active for hydrogenation reactions, yet its potential remains significantly underexplored, is metal phosphides. For example, Ni_2P has been used as a catalyst for the hydrogenation of butadiene to make butene isomers, hydrodesulfurization, carbonyl reduction to form alcohols from aldehydes, and nitrobenzene reduction to aniline.[3, 20-23] Nevertheless, the selectivity towards C=O reduction or aniline-based compounds are still low due to the competing hydrogenation reactions occurring within the substrate.[22-23] Efforts to improve the selectivity include altering the electronic properties of the metal phosphide by chemical anchoring to a support.[3] However, the electronic properties can also be altered synthetically through the addition of another metal to form a bimetallic phosphide.[24-25]

Previously, we reported bimetallic RuMoP exhibited high ring hydrogenation selectivity (99%) towards cyclohexanol at low reaction temperature (125°C).[25] Using experiments and theory, the Lewis acidic nature of RuMoP was responsible for aromatic ring adsorption and the resulting ring hydrogenation.[26] However, product selectivity is not only dependent on the nature of the active sites but also the electronic distribution of the reactant.[12] In phenol, the hydroxyl group acts as an electron donator to the aromatic ring, causing the ring to become more electron rich, which could contribute to the preferential adsorption of the ring on the surface. Therefore, variation of the functional group can alter the interaction between the reactant and the surface.

The scope of this work includes the examination of RuMoP as a catalyst for chemoselective hydrogenation of aromatic hydrocarbons with either electron withdrawing or electron donating groups. The catalytic performance of RuMoP is also studied for aromatic hydrocarbons containing multiple substituents. Additionally, the surface interaction between the substrates and the catalyst surface is probed using diffuse reflectance infrared Fourier transform spectroscopy (DRIFTS) to gain insight to the coordination environment of competing functionalities.

2. Materials and methods

2.1. Materials

Citric acid monohydrate (Amresco, 99%), $(NH_4)_6Mo_7O_{24}{\cdot}4H_2O$ (Alfa Aesar, 99%), $(NH_4)_2HPO_4$ (Amresco, 99%), $RuCl_3{\cdot}xH_2O$ (Oakwood Chemicals, 99%), KBr (Alfa Aesar, 99%), isopropanol (J.T. Baker, 99.5%), nitrobenzene (Alfa Aesar, 99%), aniline (Sigma Aldrich, 99%), benzaldehyde (Sigma Aldrich, 99.5%), toluene (Macron, 99.5%), benzyl alcohol (Alfa Aesar, 99%), phenol (Sigma Aldrich, 99%), cyclohexanol (Alfa Aesar, 99%), anisole (Alfa Aesar, 99%), methylcyclohexane (TCI Chemicals, 99%), methyl benzoate (Alfa Aesar, 99%), p-nitroanisole

(Sigma Aldrich, 97%), p-nitrophenol (TCI, 99%), n-decane (Alfa Aesar, 99%), H_2 (Airgas, 99.999%), N_2 (Airgas, 99.998%), 30%CO in He (Airgas, 99.99%), 1%O_2 in He (Airgas, 99.99%)

2.2. Catalyst synthesis and characterization

The RuMoP catalyst used in this study was synthesized according to the synthetic methods developed in our group as described previously.[25-26] In a typical synthesis, 7 mmol of citric acid was added to 50 mL of deionized water. After the citric acid was dissolved, 1.2 mmol of $(NH_4)_6Mo_7O_{24}{\cdot}4H_2O$ was dissolved in the same solution followed by the addition of 5 mmol $RuCl_3{\cdot}xH_2O$ and 5 mmol $(NH_4)_2HPO_4$. After stirring for one hour, the solution was evaporated to approximately 25 mL using a rotary evaporator. The resulting slurry was subsequently dried at 200°C for 2 h at 1°C/min ramp rate. The cake formed after drying was then ground and calcined at 550°C for 6 h with a 1°C/min ramp rate. After the calcination step, the powder was reduced under 160 mL/min H_2 flow at 650°C for 2 h with 5°C/min ramp rate. The resulting powder was pyrophoric and thus a passivation step using 160 mL/min of 1%O_2 in He for 1 h was performed before transferring the sample into a N_2 dry box for storage.

The crystal structure was confirmed using a Bruker D8 Advance Davinci powder x-ray diffractometer (XRD). The diffraction pattern was collected between 20° - 60° 2θ with a 0.02° step size, a scanning speed of 2 s per step, and a 15°/min rotation using ~50 mg sample with no further pretreatment. The Brunauer–Emmett–Teller (BET) surface area of the material was measured using a Quantachrome NOVA 2000e N_2 physisorption instrument. Prior to the analysis, ~0.25 g the sample as degassed for >12 hours under vacuum at 125°C. The composition of the metals was quantified with an Optima 8000 inductively coupled plasma – optical emission spectroscopy (ICP-OES) instrument with external calibration. The active site of the catalyst was titrated using a

Micromeritics Chemisorb 2750 with CO pulse chemisorption experiment. The sample (~0.2 g) was pretreated under 30 mL/min of H_2 at 400°C for 2 h followed by 30 mL/min of He at 400°C for 1.5 h. The last pretreatment step was at 100°C at 30 mL/min H_2 flow to prevent polycarbonyl formation.[27] The CO pulse injections were performed at 35°C with 0.1 mL injections.

The nature of the surface sites in RuMoP was probed using a Bruker Vertex 70 equipped with a Harrick Praying Mantis high pressure cell for diffuse reflectance infrared Fourier transform spectroscopy (DRIFTS) measurements. The detector used in this study was a mercury-cadmium-telluride (MCT) detector cooled with liquid N_2. The sample cup was packed with 80 mg of KBr, and 20 mg of the RuMoP powder was added as the top layer. The sample was lightly pressed to form a relatively flat surface. Prior to analysis, pure RuMoP was reduced *in situ* with 30 mL/min H_2 flow at 400°C for 2 h. After the pretreatment, the material was cooled down under a 30 mL/min flow of N_2 and background scans were collected simultaneously at 400°C, 300°C, 200°C, 100°C and 50°C. Pyridine was used as a probe molecule for the surface acid sites and was exposed to the catalyst by flowing N_2 through a pyridine bubbler maintained at room temperature for 1 hr. After saturation with pyridine, the cell was flushed with N_2 for 10 mins and spectra were collected at different temperatures using 4 cm^{-1} resolution with the appropriate background scans collected during cooling. The procedure was repeated using other adsorbates such as nitrobenzene, anisole, isopropanol, and p-nitroanisole using fresh catalysts for each experiment. The saturation temperature for these adsorbates was 100°C.

2.3. Catalyst testing

The catalyst was tested in both flow and batch reactor configurations. The flow reaction was conducted in an up-flow quarter inch 316 stainless steel tube equipped with a 10 μm stainless steel mesh screen at the top to prevent the catalyst from moving downstream from the reaction zone. In a

typical experiment, 50.0 mg of 60-100 mesh SiO_2 gel was loaded into the reactor followed with 120.0 mg SiO_2 gel mixed with 30.0 mg of RuMoP and 25.0 mg of SiO_2. The bottom of the catalyst bed was held using 10.0 mg of quartz wool. Two thermocouples were installed on top and bottom of the reactor bed to ensure temperature control throughout the catalyst bed. The catalyst was pre-treated at 400°C for 1 h under 100 mL/min of H_2 flow and cooled down to reaction temperature (125°C) rapidly. After the desired temperature was reached, the reactor was pressurized to 4.1 MPa H_2, and the liquid feed (0.02 M reactant in isopropanol) was flowed at 1.2 mL/min – 0.2 mL/min. After the reaction reached steady state, three consecutive liquid samples were taken and analyzed using an Agilent Gas Chromatograph 7890A – Mass Spectrometer 5975C (GCMS) with an external calibration. The reaction result is reported as a function of W/F defined in Equation 1 where g_{cat} is the mass of catalyst (g), N_{CO} is the moles of CO-accessible sites in RuMoP per gram (mol/g) and $F_{reactant}$ is the molar flowrate of the reactant (mol/s).

$$\frac{W}{F} = \frac{m_{cat} N_{CO}}{F_{reactant}} \tag{1}$$

A batch reactor was used for reactions that were slower, required more catalyst, or required a longer reaction time. In a typical experiment, 40.0 mg of RuMoP was loaded into a 300 mL high pressure Parr batch reactor followed immediately by the addition of 40 mL of 0.02 M reactant in isopropanol. The reactor was sealed and purged three times with 4.1 MPa N_2 followed by three purges with 4.1 MPa H_2. The reactor was heated to 125°C with a Parr 4848 temperature controller. After the reactor reached the reaction temperature, 4.1 MPa of H_2 was fed into the reactor and this point was marked as t = 0. Afterwards, 100 μL samples were taken throughout the reaction using a custom internal liquid sampler and condenser.

3. Results and discussion

3.1. Bulk and surface characterization of RuMoP

RuMoP was synthesized via temperature programmed reduction, as described in the previous section, to form the orthorhombic crystal structure confirmed by powder XRD (Figure 1). The diffraction pattern matches the reference data with (112), (211), (301), (020), (111), and (102) planes observed. The XRD pattern of orthorhombic RuMoP is distinct from patterns associated with monometallic MoP (PDF 04-002-4743), Mo_3P (PDF 03-065-1609), and RuP (PDF 04-004-3077). Using a Si(111) standard during analysis, orthorhombic Ru_2P (PDF 04-004-4140) was not observed because the peak position of RuMoP(112) was shifted to 37.9° 2θ due to the incorporation of Mo into the lattice. Ru_2P(211), however, is located at 38.2° 2θ. The shift to a smaller 2θ indicates a larger unit cell due to the incorporation of Mo. Moreover, the XRD pattern lacks peaks associated with Ru_2P (e.g., 40.6° 2θ). Therefore, the diffraction pattern in Figure 1 is associated to RuMoP. Additionally, ICP-OES was used to determine the bulk composition of the unsupported RuMoP powder, which provided a composition for Ru:Mo:P of 1.02: 0.99: 1.00. The number of CO sites determined with CO pulse chemisorption was determined as 20 μmol/g, and the BET surface area of the material was 12 m^2/g, which is in agreement with literature reports on unsupported phosphides.[24-25]

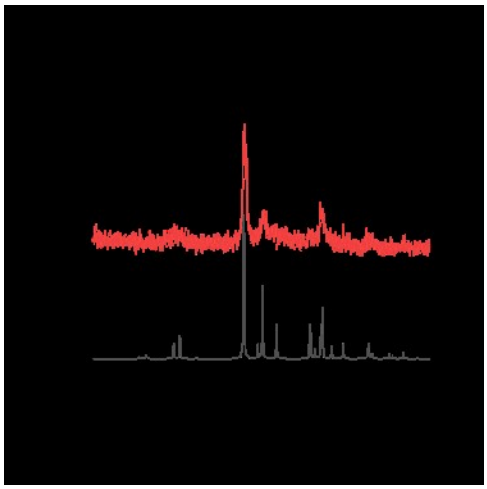

Figure 1. Diffraction pattern of RuMoP sample (red) in comparison to its reference pattern PDF 04-015-7732 (black)

The nature of the acid sites (Brønsted vs. Lewis acidity) in RuMoP was probed using DRIFTS of adsorbed pyridine serving as the probe molecule. Lewis acid sites present on the phosphide surface coordinatively bind to the N lone pair of pyridine, while Brønsted acid sites protonate the pyridine to form features characteristic of the pyridinium ion. The features associated with pyridine adsorption on Lewis acid sites (i.e., partially oxidized metal sites) were expected in the 1600-1633 cm^{-1}, 1488-1503 cm^{-1}, and 1447-1460 cm^{-1} regions.[28-31] The Brønsted acidity resulting from surface P_xO_y-H species were expected in the ~1640 cm^{-1}, 1540 cm^{-1}, and 1485-1500 cm^{-1} regions.[28-31] The pretreatment and spectra collection procedure are described in section 2.2. The spectrum collected for the pyridine saturated RuMoP surface at 50°C is shown in Figure 2a. From this spectrum, physisorbed pyridine features are observed at 1440 cm^{-1}, 1572 cm^{-1}, and 1580 cm^{-1}, which correspond to ν[CC(N)] type 19b, 8b, and 8a vibration modes in pyridine, respectively.[29, 32] After saturation, the physisorbed pyridine was removed by flushing with N_2 for 10 mins (Figure 2b). As shown in Figure 2b, the features associated with physisorbed pyridine decrease in relative intensity compared to chemisorbed pyridine. After flushing for 30 mins, the relative intensity of the physisorbed peaks decrease further (Figure 2c), revealing mainly chemisorbed species. The

decrease in relative intensity is even more apparent as the temperature is increased to 100°C and 200°C (Figure 2d, 2e). The interaction between pyridine and surface Lewis acid sites is observed from the ν[CC(N)] type 19b and 8a vibration at 1448 cm^{-1} and 1610 cm^{-1}, respectively.[32-34] The peak at 1488 cm^{-1} is assigned to both Lewis and Brønsted acid interactions, but the absence of the ν[(CC(N)] type 19b Brønsted acid feature at 1545 cm^{-1} indicates the primary adsorption mode between pyridine and RuMoP occurs from Lewis acid-type interactions.[34]

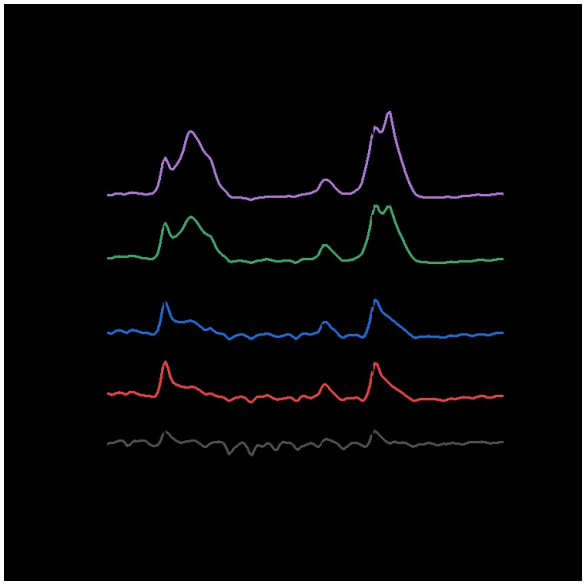

Figure 2. DRIFT spectra of pyridine adsorption at (a) saturation point, (b) after purging with N_2 at 50°C for 10 mins, (c) 50°C for 30 mins, (d) 100°C for 30 mins, and (e) 200°C for 30 mins. The dotted lines indicate pyridine adsorption on Lewis acid (L) and Brønsted acid (B).

3.2. Aromatics possessing electron withdrawing substituents

To study the hydrogenation performance of RuMoP towards the electron withdrawing group on the aromatic ring, several functionalities such as nitro, aldehyde, ketone, ester, acid, and nitrile were examined. The molecules of interest in this study are summarized in Scheme 1. For nitrobenzene (Scheme 1a), due to the N lone pair sharing with the two O attached, the N lone pair cannot be

donated back into the ring, making NO_2 a strong withdrawing group.[2] Figure 3a shows the conversion (black) and selectivity (red) to aniline for nitrobenzene hydrogenation with varying W/F. As expected, the reaction proceeds with high selectivity towards aniline (>99%) with no ring hydrogenation product being observed even at complete conversion (Figure 3a). The high selectivity of nitrobenzene to aniline was also observed with nickel phosphide using $NaBH_4$ as the H-source.[23] Here, we show the high selectivity towards aniline can also be achieved with gaseous molecular hydrogen, which is a cleaner H-source. Moreover, it has been suggested that nitrobenzene adsorption on the phosphide surface occurs through the -NO_2 group, which is discussed in more detail in Section 3.4.[23]

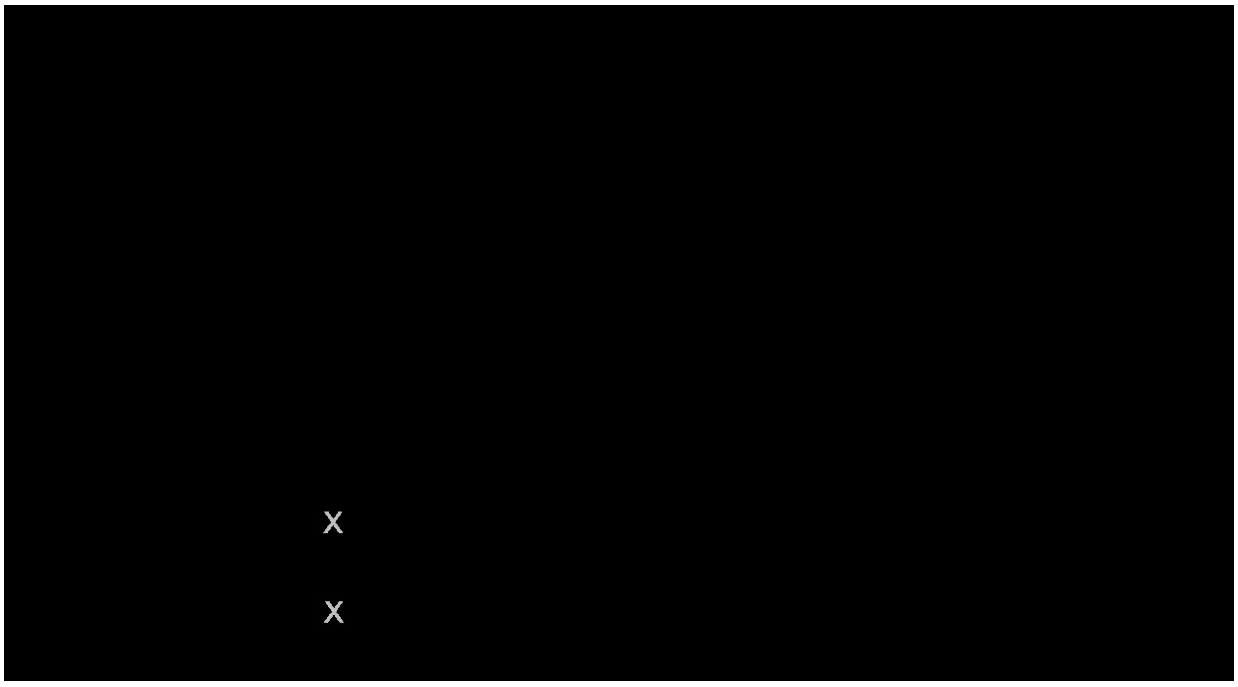

Scheme 1. Reaction summary for the hydrogenation of substituted aromatics using RuMoP with the corresponding major products at 125°C and 4.1 MPa.

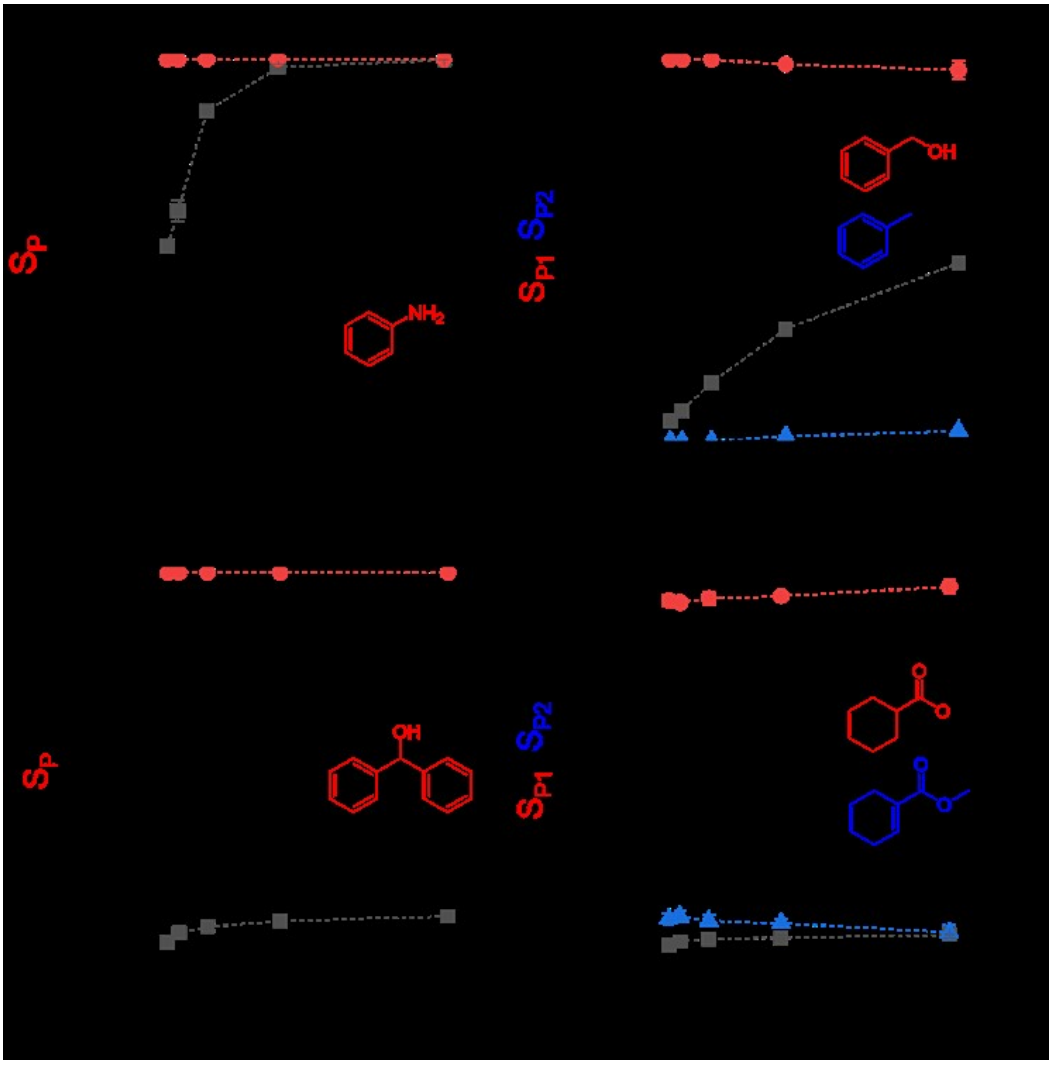

Figure 3. Conversion (black) and product selectivity (red, blue) of (a) nitrobenzene, (b) benzaldehyde, (c) benzophenone, and (d) methyl benzoate as a function of W/F.

The reduction of an aldehyde functionality to the corresponding primary alcohol was observed through benzaldehyde hydrogenation with RuMoP (Scheme 1b). The reaction result is shown in Figure 3b with conversion, selectivity to benzyl alcohol, and selectivity to toluene represented in black, red, and blue, respectively. According to the reaction result, RuMoP shows high selectivity

towards benzyl alcohol (~99%) up until 30% conversion. Small amounts of toluene were observed past this conversion, which lowered the selectivity to ~97% at 48% conversion. Interestingly, it is reported that monometallic ruthenium phosphide Ru_xP participates in C-C bond cleavage of benzaldehyde to form benzene.[35] Similar C-C bond cleavage was also reported in furan hydrodeoxygenation to form C3 and C4 products.[36] In this work, under the reaction conditions studied with RuMoP, no C-C bond cleavage was observed, which potentially suggests that the incorporation of Mo facilitates charge transfer and alters the electronic properties of the surface resulting in a weaker interaction between the substrates and the catalyst surface. Additionally, density functional theory (DFT) studies have calculated Mo as slightly positive in RuMoP, which suggests its role as the Lewis acid source needed for the required surface interaction.[26] The Lewis acidity character of RuMoP is corroborated from the DRIFTS study using pyridine, where Lewis acid binding sites were apparent in the spectra.

Ketone hydrogenation to the corresponding alcohol could also occur on RuMoP since the catalyst could reduce the carbonyl in benzaldehyde. Therefore, benzophenone was used as a substrate in the reaction (Scheme 1c). Indeed, the hydrogenation of benzophenone yields diphenylmethanol with 99% selectivity, reducing only the carbonyl group (Figure 3c). The conversion is, however, low compared to benzaldehyde hydrogenation, which is likely due to steric effects from the two benzene rings. Other solid catalysts have also been studied for selective reduction of carbonyl compounds includes oxides, zeolites, and supported metals.[12] Specifically, metals such as supported Pt, Au, Rh, Ni, Ag, Ir, and Os have been studied for selective carbonyl reduction with Os/SiO_2 providing > 99% selectivity at 5 % conversion.[12, 37] For Pt-based catalysts, selectivity to C=O reduction can be tuned by varying the support, particle size, or addition of other metals.[12, 38-39]

Although RuMoP is able to reduce the electron withdrawing group functionality in aromatic compounds containing nitro groups, aldehydes, and ketones, RuMoP cannot reduce methyl benzoate (aromatic ester; Scheme 1d) under the conditions tested in this study (125°C and 4.1 MPa). Figure 3d depicts the conversion of methyl benzoate represented in black, the selectivity of methyl cyclohexanoate in red, and the selectivity of methyl 1-cyclohenecarboxylate in blue. The hydrogenation of methyl benzoate results in the reduction of the phenyl ring to form methyl cyclohexanoate and methyl 1-cyclohexenecarboxylate, with the former being the more dominant product. Interestingly, RuMoP is not active for carboxylic acid (i.e. 3,5-dicarboxylic acid) hydrogenation at the same reaction condition. In the reduction of carboxylic acids and ester to alcohols, two steps must occur: hydrogenation of the C=O bond followed by hydrogenolysis of one of the C-O bonds.[40] However, the reaction temperature in this work is too low to overcome the C-O bond cleavage barrier. This was shown previously on RuMoP catalyst where the catalyst could not cleave C-O bond in cyclohexanol at less than 225°C.[25]

Lastly, RuMoP was inactive for benzonitrile hydrogenation at the reaction condition of 125°C and 4.1 MPa H_2. However, another bimetallic phosphide, FeMoP, was shown to be active for benzonitrile reduction at 400°C to for benzylamine and toluene.[41] Thus, the hydrogenation of benzonitrile was examined at a higher temperature of 400°C using 0.02 M of benzonitrile in n-decane as a solvent to keep the reaction in the liquid phase in the batch reactor. At 80% conversion of benzonitrile, the selectivity of the reaction was 63% benzylamine, 27% toluene, and 10% methylcyclohexane, and provides evidence that that the nitrile group can be reduced at higher reaction temperature, although other side reactions are also present.[41-42]

3.3. Aromatics possessing electron donating substituents

The effects of electron donating groups were investigated through the hydrogenation of phenol, anisole, and toluene, which contain hydroxyl, ether, and methyl groups, respectively (Scheme 1g-i). The initial assessment of these reactions was performed in a flow reactor with the same reaction conditions as the other substrates (0.02 M reactant in isopropanol, 125°C, 4.1 MPa H_2). However, no reaction was observed due to the limitation of the flow reactor bed size. Therefore, a batch reactor was used to allow for longer reaction time.

Figure 4 summarizes the reaction results for phenol, anisole, and toluene hydrogenation represented as black squares, red circles, and blue triangles, respectively. The first three points were unquantifiable due to the small peak areas lower than the external calibration. The first quantifiable peak was observed after 60 mins of reaction time. For all three reactions, the selectivity of the reaction was dominated (99%) by ring hydrogenation products. However, the conversion can be considered low compared to the substrates with electron withdrawing groups. The low conversion could possibly indicate preferential binding between the lone pair electrons in the solvent (isopropanol) in comparison to the π-electrons in the aromatic rings. Although phenol and anisole both have lone pair of electrons, electron density is donated to the aromatic ring, resulting in an alternative binding configuration with the Lewis acidic surface. A study on electron charge distribution on aromatics showed that the charge of the carbon in the phenyl ring increased from -0.037*e* to -0.100*e*, -0.131*e,* and -0.115*e* on the two ortho and para positions in phenol respectively.[43] The change in charge distribution shows electron donation from the hydoxy group in phenol. Nevertheless, the most electron rich atom in phenol is the hydroxyl O with charge of -0.686*e,* which suggests that the lone pair electrons could also bind to the electron deficient sites, but the reaction conditions are not sufficient for C-O bond cleavage.[25, 41, 43] The low conversion could possibly indicate preferential binding between the lone pair electrons in the solvent

(isopropanol) in comparison to the π-electrons in the aromatic rings. Although phenol and anisole both have lone pair of electrons, electron density is donated to the aromatic ring, resulting in an alternative binding configuration with the Lewis acidic surface. Other noble metal catalysts such as Pd, Pt, and Ru are also shown to hydrogenate the aromatic rings for phenol hydrogenation reactions to form cyclohexanone and cyclohexanol.[44-47] These catalysts can be manipulated by changing the support material to obtain C-O bond cleavage products.[45]

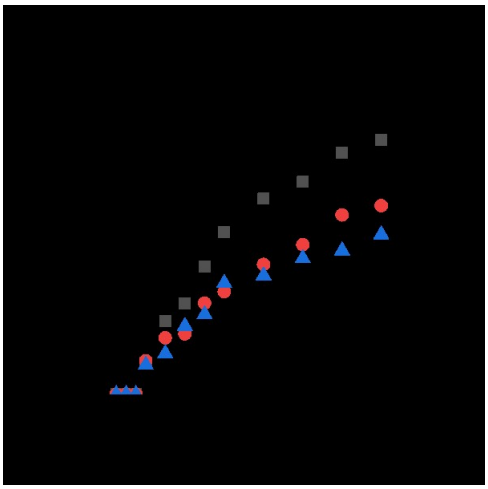

Figure 4. Conversion of phenol (black square), anisole (red circle), and toluene (blue triangle) hydrogenation reactions.

The hydrogenation of phenol to cyclohexanol can occur through cyclohexenol formation that isomerizes quickly into cyclohexanone.[44] The cyclohexanone is further hydrogenated into cyclohexanol. This pathway is often observed when the aromatic ring adsorbs planar on the surface, which is discussed more in the following section.[48-49] However, in the reaction system, no cyclohexanone was observed. The cyclohexanol formation would imply that the interaction

between phenol and the surface is through the aromatic ring and not through the lone pair of the hydroxyl O.

3.4. Substrates possessing both electron withdrawing and donating groups

Based on the results presented in the previous two sections, substrates containing multiple functionalities were studied to observe any competition for surface reactivity between the two groups. The first substrate studied was terephthalaldehyde (Scheme 1j), which contains two aldehyde groups in the para position of the aromatic ring. In this experiment, we were interested in understanding how RuMoP would interact with a molecule with the two aldehyde groups and if it would reduce only one of the aldehyde groups. Figure 5a shows the reaction results from terephthalaldehyde hydrogenation in the flow reactor where the conversion is represented in black, selectivity to p-hydroxymethylbenzaldehyde in red, and p-benzenemethanol in blue. A W/F study shows that 100% conversion can be achieved at longer residence times. However, the selectivity cannot be controlled to only one aldehyde group. Ultimately, both of the aldehyde groups are hydrogenated to form primarily p-benzenemethanol.

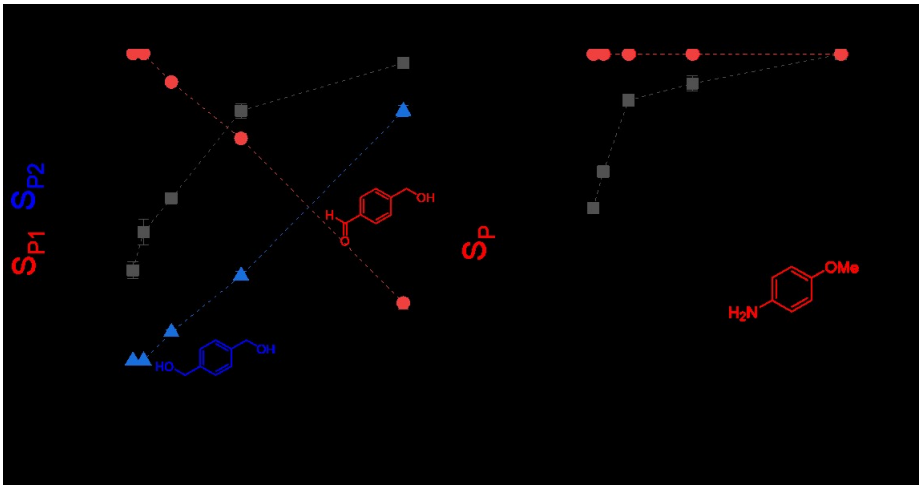

Figure 5. Conversion (black) and product selectivity (red, blue) for hydrogenation of (a) p-nitroanisole and (b) terephthalaldehyde as a function of W/F.

Additionally, the hydrogenation of substrates containing both an electron donating and an electron withdrawing group (i.e. p-nitroanisole) was also studied (Scheme 1k). The reaction result for p-nitroanisole hydrogenation is summarized in Figure 5b where the conversion is represented in black and the selectivity to p-methoxyaniline is in red. Indeed, the hydrogenation selectivity was targeted to the electron withdrawing group to form p-methoxyaniline. At 100% conversion, the selectivity is unaffected and forms only p-methoxyaniline. Although both $-NH_2$ and $-OCH_3$ are electron donating groups, the ring hydrogenation product is not observed. Other Ru-based catalysts such bimetallic Ru*M* (*M* = Sn, Pb, Ga, Mo, W, Re) have also been studied for nitrobenzene hydrogenation in the presence of other functionalities.[18, 50-51] In these studies, the selectivity towards nitro group reduction with Ru is improved with the addition of another metal, with some reports showing >99% selectivity to amine formation. As previously mentioned, electronic effects associated with alloying provide an alternative route to control the catalytic properties.

To investigate the selectivity towards the electron withdrawing group, a set of DRIFTS experiments were performed using various adsorbates with nitro or methoxy functionalities. The purpose of the experiments was to observe the adsorption mode of the nitro group and the methoxy group, respectively. The first substrate used was nitrobenzene (Figure 6a). After desorption of physisorbed nitrobenzene under a flow of N_2, two peaks remain at 1526 cm^{-1} for the asymmetric $\nu_{as}(NO_2)$ and 1349 cm^{-1} for the symmetric $\nu_s(NO_2)$ mode.[6, 52] The peak positions are downshifted from the $\nu_{as}(NO_2)$ and $\nu_s(NO_2)$ in gaseous nitrobenzene at 1548 cm^{-1} and 1360 cm^{-1}, respectively.[53] The downshift in the peak positions is attributed to surface adsorption. During saturation, a feature was observed at 1448 cm^{-1}, which is an indication of the 19a type aromatic ring vibration, but this feature disappeared after N_2 purging.[54-55] Since the ring vibration was not observed after purging,

nitrobenzene primarily interacts with the catalytic surface through the -NO_2 interaction as evident by the appearance of symmetric and asymmetric features of -NO_2.

Anisole adsorption experiments yield two resolved features (Figure 6b) at 1606 cm^{-1} and 1447 cm^{-1}, which correspond to the $\nu(CC_{ring})$ vibration 8a mode and the $\delta_{as}(CH_3)$ mode, respectively.[56-57] A small peak at 1489 cm^{-1} is also observed for the $\nu(CC_{ring})$ 19a vibration mode. The $\nu(CO)$ band at ~1498 cm^{-1} and ~1295 cm^{-1} are absent, which indicates the absence of O-surface interactions.[57] This observation agrees with the reaction results where the hydrogenation occurs primarily in the aromatic ring.[48] To investigate the competition between anisole adsorption and nitrobenzene, a physical mixture of anisole and nitrobenzene was chemisorbed on the surface to elucidate the dominate adsorption modes.[6] When a 1:1 molar ratio of nitrobenzene and anisole were introduced into the system, features from both nitrobenzene and anisole were observed (Figure 6c). Therefore, simultaneous adsorption is possible; however, this result does not provide preferential adsorption between the functionalities and the surface.

The adsorption of p-nitroanisole was also observed via DRIFTS. Because p-nitroanisole is a solid, isopropanol is used to dissolve p-nitroanisole. The features associated with isopropanol adsorption include peaks in the 1445 cm^{-1} region that correspond to $\delta_{as}(CH_3)$ similar to one observed in anisole.[58-59] Additionally, the 1608 cm^{-1} vibration was assigned to a C=C vibration that is similar to the observed C=C vibration in isopropanol oxidation to acetone through an enol intermediate.[60-61] This C=C bond is observed when the hydroxyl O on the isopropanol is adsorbed to the active sites and form a pseudo C=C bond.[60] This result indicates that the hydroxyl O from isopropanol can interact with the active sites on the surface. After dissolving p-nitroanisole with isopropanol, the mixture was placed in the N_2 bubbler. Interestingly, more features were observed in this adsorption in comparison to the physical mixture of nitrobenzene and anisole (Figure 6e). Features at 1600 cm^{-1} and 1447 cm^{-1} are associated with either isopropanol or anisole; and the contribution from the two adsorbates cannot be deconvoluted accurately. Peaks at 1505 and 1335 cm^{-1} are assigned to the $-NO_2$. The new feature at 1490 cm^{-1} is assigned to the shifted $\nu(CC_{ring})$ from anisole. The NO_2 adsorption was shifted to a lower wavenumber, which suggests a weaker bond due to the donation from the methoxy group to the aromatic ring that can further stabilize the $-NO_2$ group. The electron donation causes the $-NO_2$ to be more electron rich, which favors adsorption to the electron deficient sites and weaken the N-O bond for subsequent reduction.

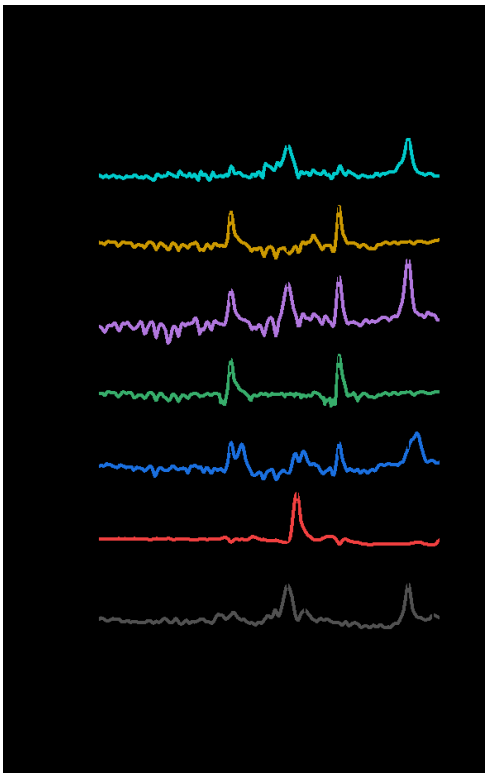

Figure 6. DRIFT spectra of chemisorbed (a) nitrobenzene, (b) anisole, (c) 1:1 molar ratio of nitrobenzene: anisole, (d) isopropanol, (e) isopropanol + p-nitroanisole, (f), isopropanol + p-nitroanisole + H_2, and (g) nitrobenzene + H_2.

Furthermore, the contribution from the H_2 was also studied with DRIFTS. The same experiment with isopropanol and p-nitroanisole was repeated, but instead of N_2, the flow was switched to H_2. After 10 mins, the spectrum in Figure 6f was observed. One major peak at 1910 cm^{-1} was observed and associated to the 19a vibration from aniline, which indicated that the reaction has proceeded and the $-NO_2$ was converted into $-NH_2$ with no additional observation of other surface intermediates. However, the adsorption on nitrobenzene in the presence of H_2 was also studied (Figure 6g). The spectrum provided new features at 1495 and 1304 cm^{-1} that correspond to the 19a and 14 vibration modes of phenylhydroxylamine, which is a reaction intermediate between nitrobenzene and aniline.[7, 52] The presence of this reaction intermediates implies that nitrobenzene is directly reduced to aniline instead of proceeding through the condensation route with azo compound formation.[7]

3.5 Solvent effects

Isopropanol is a well-known H-donator solvent. However, within this work, isopropanol cannot be solely the H-donor which is evident by the low conversion in the absence of H_2. According to our observation, the substrates with electron donating groups tend to have lower conversion in comparison to the electron withdrawing groups, which could indicate more difficult adsorption of the aromatic ring. The aromatic ring adsorption could be further hindered from the presence of the lone pair in isopropanol that competes for the adsorption sites as shown in our DRIFTS experiments. To observe this competition, n-decane was used as a solvent to avoid adsorption competition with the substrates. As shown in Figure 7, the conversion was measured as a function of time for reactions performed in a batch reactor for the hydrogenation of phenol (circle) and anisole (square). When n-decane was used as a solvent, an apparent improvement in conversion was observed as shown in Figure 7. At 420 min, the conversion was almost tripled with n-decane as the solvent in comparison to isopropanol. Similarly, anisole conversion was almost tripled when the solvent was switched to n-decane (red square). These results support the notion that competitive adsorption between the lone pair in isopropanol and the aromatic ring can influence the reactivity, and they also suggest that adsorption of isopropanol is more favorable than adsorption of the aromatic ring due the lower conversion observed in an isopropanol media. A similar observation was reported where the conversion of phenol increases in hydrocarbon solvents such as hexane in comparison to other solvents (i.e. alcohols, acetone, tetrahydrofuran, and ethyl acetate).[62-64]

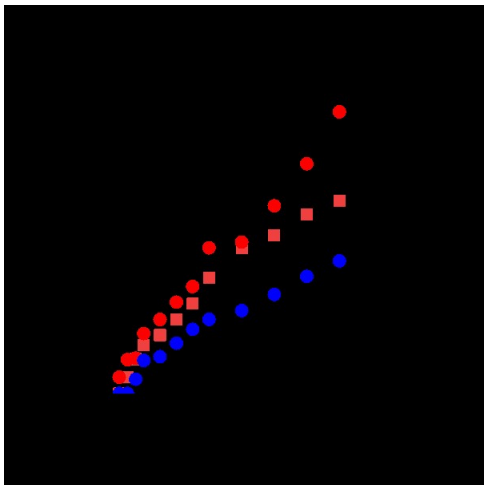

Figure 7. Solvent effects observed for phenol (circle) and anisole (square) hydrogenation in IPA (black) and n-decane (red) at 125°C and 150°C (blue) with RuMoP

4. Conclusion

In summary, the catalytic hydrogenation performance of RuMoP was evaluated with aromatics containing electron withdrawing groups, electron donating groups, and molecules containing both types of substituents. The bimetallic RuMoP catalyst can hydrogenate benzaldehyde and benzophenone to produce 1° and 2° alcohols, respectively, with 99% selectivity. Additionally, nitrobenzene is selectively reduced to aniline with 99% selectivity using RuMoP as a catalyst. Using DRIFTS, nitrobenzene adsorption in the presence of H_2 shows this reduction occurs through a direct pathway instead of a condensation route. Hydrogenation of aromatics with electron donating groups such as phenol, anisole, and toluene yield 99% selectivity to ring hydrogenation to produce cyclohexanol, methoxycyclohexane, and methyl cyclohexane, hydrogenating the electron-dense portion of the substrate. This is supported by the presence of Lewis acid sites in RuMoP, probed by pyridine adsorption in DRIFTS, which is likely to surface site participating in the hydrogenation reaction.

Author information

Corresponding author

*J. C. Hicks: jhicks3@nd.edu

Notes

The authors declare no competing financial interest

Acknowledgements

This work was supported in part by the NSF CAREER Award (CBET-1351609), Defense University Research Instrumentation Program under AFOSR Award No. FA9550-17-1-0376, a Patrick and Jana Eilers Fellowship through ND Energy, and the Bayer Center of Environmental Science & Technology (CEST) Fellowship. We would like to thank Material Characterization Facility (MCF) for the use of XRD and CEST at the University of Notre Dame for the use of the ICP-OES. VESTA software was used to draw the crystal structure of RuMoP in the TOC.[65]

References

1. Blaser, H.-U.; Malan, C.; Pugin, B.; Spindler, F.; Steiner, H.; Studer, M. Selective hydrogenation for fine chemicals: recent trends and new developments. *Adv. Synth. Catal.* **2003,** *345*, 103-151.
2. Ono, N., *The nitro group in organic synthesis*. New York : Wiley-VCH: New York, 2001.
3. Gao, R. J.; Pan, L.; Wang, H. W.; Zhang, X. W.; Wang, L.; Zou, J. J. Ultradispersed nickel phosphide on phosphorus-doped carbon with tailored d-band center for efficient and chemoselective hydrogenation of nitroarenes. *ACS Catal.* **2018,** *8*, 8420-8429.
4. Dimitriou, E.; Jones, R. H.; Pritchard, R. G.; Miller, G. J.; O'Brien, M. Gas-liquid flow hydrogenation of nitroarenes: Efficient access to a pharmaceutically relevant pyrrolobenzo[1,4]diazepine scaffold. *Tetrahedron* **2018,** *74*, 6795-6803.
5. Khilnani, V. L.; Chandalia, S. B. Selective hydrogenation. I. para-chloronitrobenzene to para-chloroaniline platinum on carbon as catalyst. *Org. Process Res. Dev.* **2001,** *5*, 257-262.
6. Boronat, M.; Concepcion, P.; Corma, A.; Gonzalez, S.; Illas, F.; Serna, P. A molecular mechanism for the chemoselective hydrogenation of substituted nitroaromatics with nanoparticles of gold on TiO2 catalysts: A cooperative effect between gold and the support. *J. Am. Chem. Soc.* **2007,** *129*, 16230-16237.
7. Corma, A.; Concepcion, P.; Serna, P. A different reaction pathway for the reduction of aromatic nitro compounds on gold catalysts. *Angew. Chem. Int. Edit.* **2007,** *46*, 7266-7269.
8. Hicks, J. C. Advances in C-O bond transformations in lignin-derived compounds for biofuels production. *J. Phys. Chem. Lett.* **2011,** *2*, 2280-2287.
9. Alonso, D. M.; Wettstein, S. G.; Dumesic, J. A. Bimetallic catalysts for upgrading of biomass to fuels and chemicals. *Chem. Soc. Rev.* **2012,** *41*, 8075-8098.
10. Bridgwater, A. V. Review of fast pyrolysis of biomass and product upgrading. *Biomass Bioenerg* **2012,** *38*, 68-94.
11. McEwan, L.; Julius, M.; Roberts, S.; Fletcher, J. C. Q. A review of the use of gold catalysts in selective hydrogenation reactions. *Gold Bull.* **2010,** *43*, 298-306.

12. Maki-Arvela, P.; Hajek, J.; Salmi, T.; Murzin, D. Y. Chemoselective hydrogenation of carbonyl compounds over heterogeneous catalysts. *Appl. Catal. A* **2005,** *292*, 1-49.
13. Wang, Y.; Yao, J.; Li, H. R.; Su, D. S.; Antonietti, M. Highly selective hydrogenation of phenol and derivatives over a Pd@carbon nitride catalyst in aqueous media. *J. Am. Chem. Soc.* **2011,** *133*, 2362-2365.
14. Gu, J.; Zhang, Z. Y.; Hu, P.; Ding, L. P.; Xue, N. H.; Peng, L. M.; Guo, X. F.; Lin, M.; Ding, W. P. Platinum nanoparticles encapsulated in MFI zeolite crystals by a two-step dry gel conversion method as a highly selective hydrogenation catalyst. *ACS Catal.* **2015,** *5*, 6893-6901.
15. Wei, H. S.; Liu, X. Y.; Wang, A. Q.; Zhang, L. L.; Qiao, B. T.; Yang, X. F.; Huang, Y. Q.; Miao, S.; Liu, J. Y.; Zhang, T. FeOx-supported platinum single-atom and pseudo-single-atom catalysts for chemoselective hydrogenation of functionalized nitroarenes. *Nat. Commun.* **2014,** *5*.
16. Kluson, P.; Cerveny, L. Selective hydrogenation over ruthenium catalysts. *Appl. Catal. A* **1995,** *128*, 13-31.
17. Hermans, S.; Raja, R.; Thomas, J. M.; Johnson, B. F. G.; Sankar, G.; Gleeson, D. Solvent-free, low-temperature, selective hydrogenation of polyenes using a bimetallic nanoparticle Ru-Sn catalyst. *Angew. Chem. Int. Edit.* **2001,** *40*, 1211.
18. Tamura, M.; Yuasa, N.; Nakagawa, Y.; Tomishige, K. Selective hydrogenation of nitroarenes to aminoarenes using a MoOx-modified Ru/SiO2 catalyst under mild conditions. *Chem. Commun.* **2017,** *53*, 3377-3380.
19. Johnstone, R. A. W.; Wilby, A. H.; Entwistle, I. D. Heterogeneous catalytic transfer hydrogenation and its relation to other methods for reduction of organic compounds. *Chem. Rev.* **1985,** *85*, 129-170.
20. Nozaki, F.; Tokumi, M. Hydrogenation activity of metal phosphides and promoting effect of oxygen. *J. Catal.* **1983,** *79*, 207-210.
21. Nozaki, F.; Kitoh, T.; Sodesawa, T. Promoting effect of oxygen for hydrogenation of butadiene over Ni2P catalyst. *J. Catal.* **1980,** *62*, 286-293.
22. Wang, H.; Shu, Y. Y.; Zheng, M. Y.; Zhang, T. Selective hydrogenation of cinnamaldehyde to hydrocinnamaldehyde over SiO(2) supported nickel phosphide catalysts. *Catal. Lett.* **2008,** *124*, 219-225.
23. Liu, K.; Wang, Y.; Chen, P.; Zhong, W. B.; Liu, Q. Z.; Li, M. F.; Wang, Y. D.; Wang, W. W.; Lu, Z. T.; Wang, D. Noncrystalline nickel phosphide decorated poly(vinyl alcohol-co-ethylene) nanofibrous membrane for catalytic hydrogenation of p-nitrophenol. *Appl. Catal. B* **2016,** *196*, 223-231.
24. Rensel, D. J.; Rouvimov, S.; Gin, M. E.; Hicks, J. C. Highly selective bimetallic FeMoP catalyst for C-O bond cleavage of aryl ethers. *J. Catal.* **2013,** *305*, 256-263.
25. Bonita, Y.; Hicks, J. C. Periodic trends from metal substitution in bimetallic Mo-based phosphides for hydrodeoxygenation and hydrogenation reactions. *J. Phys. Chem. C* **2018,** *122*, 13322-13332.
26. Jain, V.; Bonita, Y.; Brown, A.; Taconi, A.; Hicks, J. C.; Rai, N. Mechanistic insights into hydrodeoxygenation of phenol on bimetallic phosphide catalysts. *Catal. Sci. Technol.* **2018,** *8*, 4083-4096.
27. Corro, G.; Gomez, R. Carbon-monoxide adsorption and hydrogen-oxygen titration on Ru-Al2o3. *React. Kinet. Catal. Lett.* **1979,** *12*, 145-150.
28. Chakraborty, B.; Viswanathan, B. Surface acidity of MCM-41 by in situ IR studies of pyridine adsorption. *Catal. Today* **1999,** *49*, 253-260.
29. Zaki, M. I.; Hasan, M. A.; Al-Sagheer, F. A.; Pasupulety, L. In situ FTIR spectra of pyridine adsorbed on SiO2-Al2O3, TiO2, ZrO2 and CeO2: general considerations for the identification of acid sites on surfaces of finely divided metal oxides. *Colloid Surf., A* **2001,** *190*, 261-274.
30. Basila, M. R.; Kantner, T. R.; Rhee, K. H. The nature of the acidic sites on a silica-alumina. Characterization by infrared spectroscopic studies of trimethylamine and pyridine chemisorption. *J. Phys. Chem.* **1964,** *68*, 3197-3207.

31. Layman, K. A.; Ivey, M. M.; Hemminger, J. C. Pyridine adsorption and acid/base complex formation on ultrathin films of γ-Al2O3 on NiAl(100). *J. Phys. Chem. B* **2003,** *107*, 8538-8546.
32. Lee, Y. K.; Oyama, S. T. Bifunctional nature of a SiO2-supported Ni2P catalyst for hydrotreating: EXAFS and FTIR studies. *J. Catal.* **2006,** *239*, 376-389.
33. Barzetti, T.; Selli, E.; Moscotti, D.; Forni, L. Pyridine and ammonia as probes for FTIR analysis of solid acid catalysts. *J. Chem. Soc. Faraday Trans.* **1996,** *92*, 1401-1407.
34. Parry, E. P. An infrared study of pyridine adsorbed on acidic solids characterization of surface acidity. *J. Catal.* **1963,** *2*, 371-379.
35. Sampath, A.; Chang, S. A.; Flaherty, D. W. Catalytic hydrogen transfer and decarbonylation of aromatic aldehydes on Ru and Ru phosphide model catalysts. *J. Phys. Chem. C* **2018,** *122*, 23600-23609.
36. Bowker, R. H.; Smith, M. C.; Pease, M. L.; Slenkamp, K. M.; Kovarik, L.; Bussell, M. E. Synthesis and hydrodeoxygenation properties of ruthenium phosphide catalysts. *ACS Catal.* **2011,** *1*, 917-922.
37. Singh, U. K.; Vannice, M. A. Liquid-phase citral hydrogenation over SiO2-supported group VIII metals. *J. Catal.* **2001,** *199*, 73-84.
38. O'Driscoll, A.; Curtin, T.; Hernandez, W. Y.; Van Der Voort, P.; Leahy, J. J. Hydrogenation of furfural with a Pt-Sn catalyst: the suitability to sustainable industrial application. *Org. Process Res. Dev.* **2016,** *20*, 1917-1929.
39. Plomp, A. J.; Vuori, H.; Krause, A. O. I.; de Jong, K. P.; Bitter, J. H. Particle size effects for carbon nanofiber supported platinum and ruthenium catalysts for the selective hydrogenation of cinnamaldehyde. *Appl. Catal. A* **2008,** *351*, 9-15.
40. Pritchard, J.; Filonenko, G. A.; van Putten, R.; Hensen, E. J. M.; Pidko, E. A. Heterogeneous and homogeneous catalysis for the hydrogenation of carboxylic acid derivatives: history, advances and future directions. *Chem. Soc. Rev.* **2015,** *44*, 3808-3833.
41. Rensel, D. J.; Kim, J.; Jain, V.; Bonita, Y.; Rai, N.; Hicks, J. C. Composition-directed $Fe_xMo_{2-x}P$ bimetallic catalysts for hydrodeoxygenation reactions. *Catal. Sci. Technol.* **2017,** *7*, 1857-1867.
42. *The quantification of the products are challenging due to overlapping GCMS peak between benzonitrile and benzylamine*.
43. Misiaszek, T.; Szostak, M. M. Atomic charge distribution in 4-isopropylphenol molecule derived from atomic polar tensors. *J. Molec. Struct.* **2000,** *526*, 303-308.
44. Liu, H. Z.; Jiang, T.; Han, B. X.; Liang, S. G.; Zhou, Y. X. Selective phenol hydrogenation to cyclohexanone over a dual supported Pd-Lewis acid catalyst. *Science* **2009,** *326*, 1250-1252.
45. Newman, C.; Zhou, X.; Goundie, B.; Ghampson, I. T.; Pollock, R. A.; Ross, Z.; Wheeler, M. C.; Meulenberg, R. W.; Austin, R. N.; Frederick, B. G. Effects of support identity and metal dispersion in supported ruthenium hydrodeoxygenation catalysts. *Appl. Catal. A* **2014,** *477*, 64-74.
46. Li, Z.; Garedew, M.; Lam, C. H.; Jackson, J. E.; Miller, D. J.; Saffron, C. M. Mild electrocatalytic hydrogenation and hydrodeoxygenation of bio-oil derived phenolic compounds using ruthenium supported on activated carbon cloth. *Green Chem.* **2012,** *14*, 2540-2549.
47. Ohta, H.; Kobayashi, H.; Hara, K.; Fukuoka, A. Hydrodeoxygenation of phenols as lignin models under acid-free conditions with carbon-supported platinum catalysts. *Chem. Commun.* **2011,** *47*, 12209-12211.
48. Zhong, J. W.; Chen, J. Z.; Chen, L. M. Selective hydrogenation of phenol and related derivatives. *Catal. Sci. Technol.* **2014,** *4*, 3555-3569.
49. Taylor, D. R.; Ludlum, K. H. Structure and orientation of phenols chemisorbed on gamma-alumina. *J. Phys. Chem.* **1972,** *76*.
50. Coq, B.; Figueras, F. Geometric and electronic effects in the conversion of methylcyclopentane on Pt-Sn catalysts. *J. Mol. Catal.* **1984,** *25*, 87-98.
51. Chary, K. V. R.; Srikanth, C. S. Selective hydrogenation of nitrobenzene to aniline over Ru/SBA-15 catalysts. *Catal. Lett.* **2009,** *128*, 164-170.

52. Richner, G.; van Bokhoven, J. A.; Neuhold, Y. M.; Makosch, M.; Hungerbuhler, K. In situ infrared monitoring of the solid/liquid catalyst interface during the three-phase hydrogenation of nitrobenzene over nanosized Au on TiO2. *Phys. Chem. Chem. Phys.* **2011,** *13*, 12463-12471.
53. Varsányi, G.; Holly, S.; Imre, L. Some characteristic vibration patterns of the organic nitro group. *Spectrochim. Acta A* **1967,** *23*, 1205-1210.
54. Clavijo-Campos, R. E.; Weiss-López, B. Phase dependence of the IR spectra of nitrobenzene *Spectrosc. Lett.* **1990,** *23*, 137-145.
55. Meijers, S.; Ponec, V. Infrared spectroscopic study of the adsorption of nitro compounds and amines on cobalt oxide. *J. Catal.* **1994,** *149*, 307-316.
56. Gemechu, A. S.; Hoffmann, L. J. H.; Marquardt, S.; Eisenhardt, C. G.; Baumgartel, H.; Chelli, R.; Cardini, G.; Califano, S. The absorption spectrum of anisole and the anisole/CO2 1 : 1-cluster. The influence of intermolecular interaction on intramolecular vibrations. *Z. Phys. Chem.* **2004,** *218*, 123-153.
57. Popov, A.; Kondratieva, E.; Gilson, J. P.; Mariey, L.; Travert, A.; Mauge, F. IR study of the interaction of phenol with oxides and sulfided CoMo catalysts for bio-fuel hydrodeoxygenation. *Catal. Today* **2011,** *172*, 132-135.
58. Carriazo, D.; Martin, C.; Rives, V. An FT-IR study of the adsorption of isopropanol on calcined layered double hydroxides containing isopolyrnolybdate. *Catal. Today* **2007,** *126*, 153-161.
59. Martinez-Ramirez, Z.; Gonzalez-Calderon, J. A.; Almendarez-Camarillo, A.; Fierro-Gonzalez, J. C. Adsorption and dehydrogenation of 2-propanol on the surface of gamma-Al2O3-supported gold. *Surf. Sci.* **2012,** *606*, 1167-1172.
60. Li, S. Z.; Wen, M.; Chen, H.; Ni, Z. L.; Xu, J.; Shen, J. Y. Amination of isopropanol to isopropylamine over a highly basic and active Ni/LaAlSiO catalyst. *J. Catal.* **2017,** *350*, 141-148.
61. Barakat, C.; Gravejat, P.; Guaitella, O.; Thevenet, F.; Rousseau, A. Oxidation of isopropanol and acetone adsorbed on TiO2 under plasma generated ozone flow: Gas phase and adsorbed species monitoring. *Appl. Catal. B* **2014,** *147*, 302-313.
62. Feng, G.; Liu, Z.; Chen, P.; Lou, H. Influence of solvent on upgrading of phenolic compounds in pyrolysis bio-oil. *RSC Adv.* **2014,** *4*, 49924-49929.
63. Takagi, H.; Isoda, T.; Kusakabe, K.; Morooka, S. Effects of solvents on the hydrogenation of mono-aromatic compounds using noble-metal catalysts. *Energ. Fuel* **1999,** *13*, 1191-1196.
64. Wang, X.; Rinaldi, R. Solvent effects on the hydrogenolysis of diphenyl ether with Raney nickel and their Implications for the conversion of lignin. *ChemSusChem* **2012,** *5*, 1455-1466.
65. Momma, K.; Izumi, F. VESTA 3 for three-dimensional visualization of crystal, volumetric and morphology data. *J. Appl. Crystallogr.* **2011,** *44*, 1272-1276.

Table of contents (TOC) figure

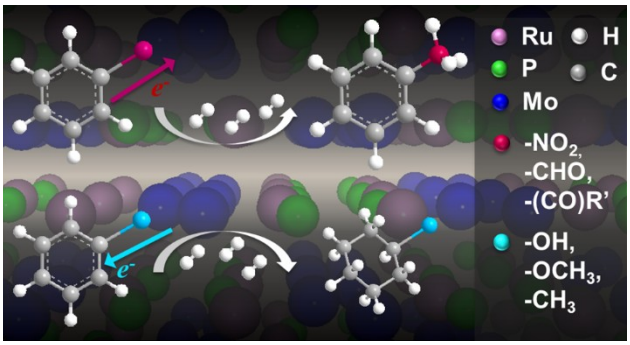
e⁻
e⁻
Ru
H
P
C
Mo
-NO2,
-CHO,
-(CO)R'
-OH,
-OCH3,
-CH3